Acta Universitatis Sapientiae
Electrical and Mechanical Engineering, 11 (2019) 99-116

DOI: 10.2478/auseme-2019-0009

Study of Powder Particle Size Effect on Microstructural and Geometrical Features of Laser Claddings Using Response Surface Methodology RSM

El Hadi BOUSSAHA[1], Samia AOUICI[2], Hamdi AOUICI[3], Abida BAHLOUL[4]

[1] Department of Petrochemistry and Process Engineering, Faculty of Technology, Université 20 Août 1955 Skikda, Algeria, e-mail: bhedi3@yahoo.fr
[2] Department of Mechanical Engineering, Faculty of Technology, Université 20 Août 1955 Skikda, Algeria, e-mail: auoici_s@yahoo.fr
[3] Higher National School of Technology, Rouiba, Algeria, e-mail: hamdi.aouici@enst.dz
[4] L.A.I.G.M. Laboratory, Faculty of Science and Technology University of Guelma, BP. 401, Algeria, e-mail: abida_bahloul@yahoo.fr

Manuscript received September 22, 2018; revised May 3, 2019

Abstract: A continuous CO2 laser (10.6 μm wavelength) was adopted to investigate the influence of powder particle sizes on microstructural and morphological characteristics of laser claddings.

To study the potential of powder in controlling the incident laser energy, different average particle sizes of Ni-base powder were deposited on an austenitic stainless steel X3CrNi18-10 substrate. The energy value necessary to melt a mass *m* of powder was calculated. The results indicate that this energy decreases with particle sizes.

The claddings obtained with small particle sizes revealed a good morphological aspect and a low dilution of the cladding layer in the substrate, yet enough to create a very good metallurgical bond. The residual stress state was also influenced. Concerning modeling, we have elaborated residual stress model in the case of laser cladding by exploiting the response surface methodology (RSM), using a quadratic regression model. Combined effects of three laser cladding parameters on the residual stress is explored by a statistical analysis of variance (ANOVA). Results show that the residual stress is influenced principally by the power delivered by laser beam and by the scanning speed. It is also indicated that the size of powder particle is the dominant factor affecting the residual stress.

Keywords: Laser cladding, particle size, energy absorption, morphology, microstructure, RSM, ANOVA.

1. Introduction

The availability of high power lasers has opened many new and diversified applications in several technological areas [1,3]. The laser cladding obtained by powder injection offers the possibility to apply a broad variety of metallurgical and ceramic coatings on the surface of materials. The Ni-Cr alloys are widely used in the glassware industry for coating parts working at high temperature in order to ensure a protection against corrosion and abrasion [4,5]. However, the quality of the coatings with regard to microstructural defects (cracking and porosity), mechanical properties (microhardness and wear resistance) and residual stresses state depends on many parameters such as laser power, powder feed rate and beam focus relative to the substrate surface and usually, no systematic study of the combined influence of these parameters was carried out. Such an investigation appears very useful for obtaining the appropriate operating conditions.

The influence of processing conditions on geometrical features of laser claddings obtained by powder injection has been studied [6,7]. However, the relationship between the powder characteristics and geometrical features of laser claddings has not been thoroughly examined.

Furthermore, it has been shown that the amount of the photonic energy participating in the resulting heating of the powder is strongly dependent on the screen opacity formed by the powder [8]. So the particle size appears like one of the predominant factors.

The aim of this work was to study the influence of particle sizes on the microstructure and morphological aspect of claddings obtained by powder injection with a continuous wave CO2 laser. Deposition is made on an austenitic stainless steel (304L). Coaxial powder injection is chosen to localize the powder flow in the previously formed cladding.

Different particle sizes of powder have been chosen in order to investigate their effects on the laser absorption and consequently on the properties of laser claddings. Concerning modeling, we have elaborated the residual stresses model in the case of laser claddings by exploiting the response surface methodology (RSM), using a quadratic regression model. Combined effects of particle sizes (d, μm), laser power (P, W) and scan speed (V, mm/s) parameters on the performance of residual substrate and deposit stress are explored by a statistical analysis of variance (ANOVA).

This article concludes with a number of suggestions for improving the quality of laser claddings.

2. Experimental procedure

2.1 Materials

A Ni-base alloy powder (PEM 133) with a particle size ranging from 20 to 120 μm was chosen as coating material (*Fig. 1*). 180×70×10 mm^3 rectangular samples of an austenitic stainless steel X3CrNi18-10 (304L) have been used as substrates. The chemical compositions (in wt. %) are listed in *Table 1*. These materials were selected because they have different machining characteristics and are important in industry [9]. Prior to the laser cladding process, the sample surface was degreased with acetone and cleaned with alcohol.

Figure 1: Optical micrograph showing particle sizes and shapes of the Ni-base powder.

Table 1: Chemical composition (wt. %) of Ni-alloy powder coating and stainless steel substrate

Elements	***C***	***B***	***Si***	***Cr***	***Fe***	***Ni***	***Mn***	***P***
Powder (PEM 133)	0.65	3.15	4.4	14	4	Balance		
X3CrNi18-10 (304L)	0.03	-	0.75	18	68.7	10	1.5	0.02

2.2 Laser claddings

Specimens were mounted on a numerically controlled X-Y table and irradiated with a continuous wave CO2 laser (10.6 μm wavelength), the power of which can reach 3.6 kW.

A 191 mm focal-length lens was employed to focus the beam at a distance of 20 mm away from the specimen surface. The claddings were achieved by

spraying alloy powders using a Metco 4 MP spray system. Argon was used to prevent oxidation and protect the alloy powder which was injected towards the molten pool via a coaxial nozzle (*Fig. 2*).

The parameters used for the treatments were as follows:

Laser power: 1500 < P < 2200 W; scanning speed: 5 < V < 10 mms-1; beam diameter at the impinging point: 1.5 < db < 2 mm.

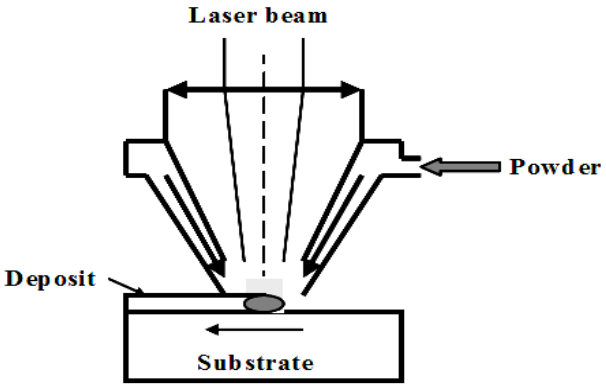

Figure 2: Coaxial nozzle.

2.3 Characterization

Following laser irradiation, the treated zones were characterized using optical microscopy (Leitz Metallovert). Scanning electron microscope (JEOL. 840-LGS) was used to study the morphology of the claddings. For optical micrography, samples were cut with a diamond grinding wheel, polished with abrasive paper, then with diamond paste and etched in the following reagent: 150 cm3 HCl, 25 g K2Cr3O7, 50 cm3 H2O.

The residual stress fields were obtained by measuring the deformation resulting from the successive removal of thin layers [10, 11]. This method so-called bending deflection method doesn't generate any stresses [12].

3. Results and discussion

The thermo-physical data and mechanical properties of most alloys are poorly known, especially at high temperature. In addition, the high thermal gradients and cooling rates generated during laser treatment render difficult an estimation of the phase transformations [12, 13]. Therefore, only qualitative trends will be discussed below.

3.1 Energy statement

When the laser beam has irradiated the surface of material, long enough, the surface temperature reaches the melting temperature (T_M). The material begins to absorb the latent heat of fusion (ΔH_M) and a molten liquid-solid interface propagates into the material. The minimum energy required to melt a mass, *m* of this material is given by:

$$E = m\left(c\Delta T + \Delta H_M\right), \tag{1}$$

with $\Delta T = T_M - T_0$, where T_0 is the initial temperature and *c* is the specific heat capacity.

In the present study; the main compounds of the powders are iron, nickel and chromium. These transition elements have similar properties [14]. Then these elements can be considered to have the following average values of the parameters.

ρ = 8000 kg m^{-3}, c = 0.5 kJ·kg^{-1}·°K^{-1}, ΔH_M = 250 kJ·kg^{-1}, T_M = 1500 °C.

So, melting 1g of material requires approximately 1000J. However, this value has to be modified since the efficiency γ of the laser cladding process is lower than 100% and part of the energy is reflected by the powder. This rate is characterized by the reflectivity *R*.

In this investigation, both factors have been taken into account. Assuming that *R* does not change significantly before the surface reaches its melting point, the minimum energy becomes:

$$E = 1000\frac{F\gamma}{(1-R)}, \tag{2}$$

where F is the powder feed rate, 1-R=A is the coefficient of absorptivity, and E is expressed in J·g^{-1}· s^{-1}.

3.2 Effect of particle size on the thermodynamic properties

If powder particles are assumed to be spheres, then the minimum energy required for melting a particle with an average radius r_p and a mass density ρ is described by the equation:

$$E_p = \frac{4}{3}\pi\rho\left(r_p\right)^3\left[c\Delta T + \Delta H_m\right] \tag{3}$$

For example, the amount of energy required to melt large particle size (r_p = 50 μm) is about 125 times larger than the amount that would have been required by small ones (r_p = 10 μm) and consequently we can see the effect of particle size on the thermodynamic properties of materials, especially the

amount of energy required for melting a small particle size smaller than that of larger size. Physically, this means the absorption of laser energy is a much localized surface phenomenon. The reduction in the size of the particle for a given powder mass leads to a multiplication of these surfaces and consequently to an increase in the resulting absorption.

3.3 Effect of particle size on the screen opacity

The reflectance *R* of the surface is an important factor. It defines how much of the energy incident on the surface is reflected. Reflected energy, of course, does not contribute to the heating. In the present case this assumption appears realistic, since the average dimensions of powder particles are large enough. Therefore, the absorptivity is essentially equal to (1-*R*).

In practice as we have seen above the minimum energy does change significantly with the particle sizes. When the particle size is large enough (average particle size: r_p = 50 μm), the powder forms a dispersed particle screen for the incident laser beam, which interacts only once with each particle. Consequently, only a small fraction of the incident energy is absorbed by the powder. Whereas, small particle size (average particle size: r_p = 15 μm) induces a concentrated screen, within which each particle is submitted to a multiple scattering phenomenon (*Fig. 3*).

This phenomenon leads to an increase in absorption and then to a better efficiency of the laser cladding process.

A simple observation indicates that if the laser beam interacts *n* times with particles the absorbed energy is no longer *E* (1-R) but *E* (1-R^n). Taking for example γ = 30%, *F* = 30 g·min^{-1} =(0.5 g s^{-1}), and *R* = 50%, we obtain for large particles (*n* = 1): *E* = 300 J and for small ones (n = 2): *E* = 450 J. The amount of energy absorbed by small particles (r_p = 10 μm) is about 1.5 times larger than the amount that would have been absorbed by the particles with great dimensions (r_p = 50 μm).

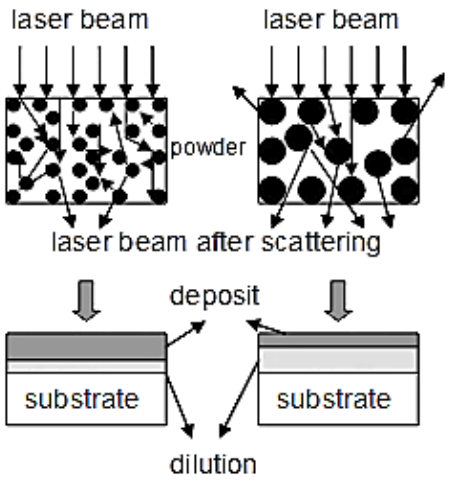

(a) Small particle size (b) Dispersed particle screen

Figure 3: Schematic illustration showing the multiple scattering phenomenon within the screen formed by the powder and its effect on the geometrical characteristics of the cladding. (a) small particle size, (b) dispersed particle screen.

4. Laser claddings properties

4.1 Morphological aspect and dilution rate

The dilution rate is defined as the ratio of the thickness of the cladding layer to the total thickness in which melting occurred. *Fig. 4* shows the optical micrograph of the cladding layers formed with different particle sizes at a laser power of 1600 W and a scan speed of 6.6 mm s^{-1}. The thickness of coatings was about 1.5 mm. The clad layer obtained with small particle size presents a good morphological aspect with a low dilution rate (*Fig.4a*). While the cladding obtained with large particle sizes shows a very high dilution with partially molten particles at the top surface (*Fig.4b*). This is probably due to the fact that during the flight through the laser beam, large particles are heated or only partially molten. Melting occurs when the powder reaches the melt zone that has been initiated on the substrate.

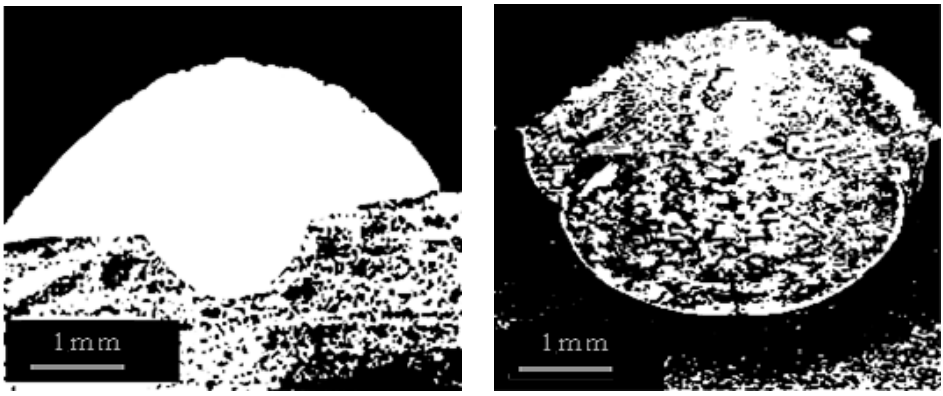

Figure 4: Optical micrographs showing the morphological aspect and the dilution rate of the clad layer: a) small particle size, b) large particle size.

The small particles are melted by the laser beam before reaching the melting zone (Figure 5), which gives a good morphological appearance of the coating while using the optimized parameters of the treatment

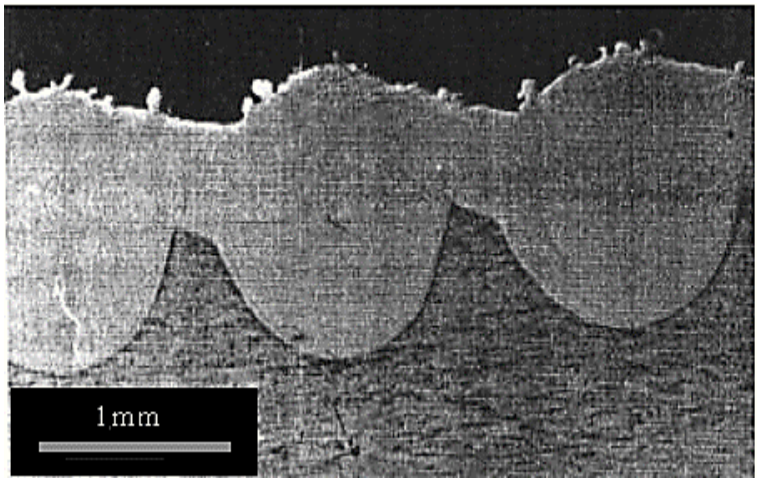

Figure 5: Optical micrograph showing the overlapping passes which resulted in coating.

4.2 Microstructure

The claddings obtained with different particles sizes revealed a cellular and dendritic microstructure which is typical of laser cladding. However, the microstructure of the cladding layer obtained with small particles size showed

columnar growth traversing the cross section (*Fig.6*). In addition, a region with a thickness of few micrometers, corresponding to planar front growth was also observed at the interface between the substrate and the cladding layer. This is may be attributed to the effect of the particle size on the solidification rate and thermal gradients.

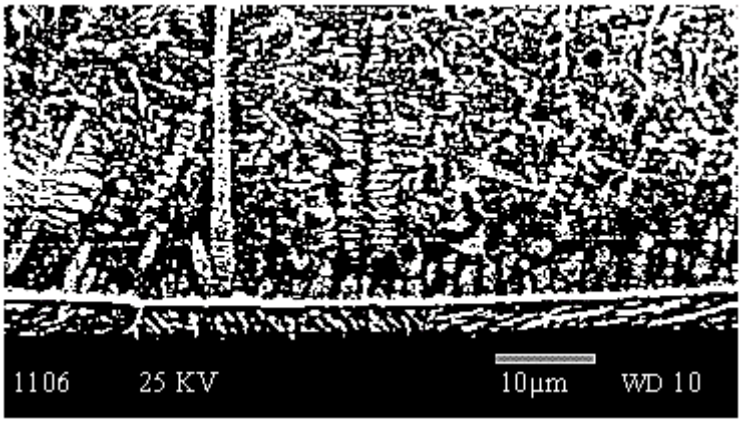

Figure 6: SEM micrograph showing the typical microstructure of the clad layer obtained with small particle sizes: directional solidification from a planar interface.

4.3 Residual stress state

It was observed (*Fig.7*) on residual stress profiles of the coatings obtained with different particle sizes on an austenitic stainless steel substrate, that the form of the stress distribution is not affected by the change of the particle size: high tensile stresses in the coating followed by a rapid decrease in compression at the interface coating/base material. However, the magnitude of these stresses decreases with the particle size. The claddings obtained with small size particles result in moderate tensile stresses in the surface and subsurface regions, with a smooth transition from tension to compression with depth.

These differences may be attributed to thermal cycles much faster and higher for the great particles than those obtained with small ones.

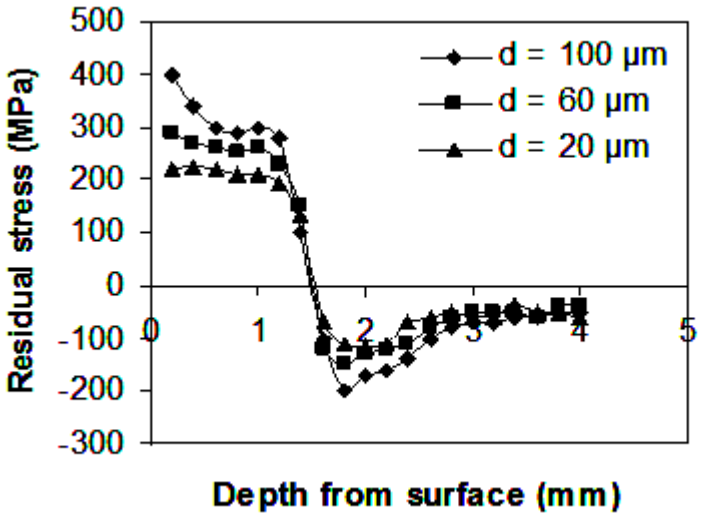

Figure 7: Residual stress fields of Ni-alloy coatings on stainless steel substrate for different average particle sizes, *d.*

5. Statistical analysis

5.1 Response surface methodology

Response surface methodology is an experimental technique used for predicting and modeling complicated relations between independent factors and one or more responses. In addition, the performance of RSM which is a well-recognized method in finding optimum condition is evaluated for finding optimal values of cutting parameters to minimize the values of cutting force components. To achieve these aims the following steps are designated: (1) defining the independent input variables and the desired output responses, (2) adopting an experimental design plan, (3) performing regression analysis with the quadratic regression models of RSM, (4) calculating the ANOVA for the independent input variables in order to find parameters which significantly affect the response, (5) determining the situation of quadratic regression models of RSM and finally, (6) optimizing, conducting confirmation experiment and verifying the predicted performance characteristics [15].

In our study particle sizes (d, µm) (diameter of the particle), laser power (P, W) and scan speed (V, mm/s) have been chosen as process parameters. The residual stresses have been chosen as response factor.

The relationship between the input parameters and the output parameters is given:

$$Y = \phi(S, P, V), \tag{4}$$

where Y is the desired the microstructural and geometrical aspect and is the response function. The approximation of Y is proposed by using a multiple linear mathematical model, which is suitable for studying the interaction effects of process parameters on microstructural and geometrical characteristics. In the present work, the RSM based multiple linear mathematical model is given by the following:

$$Y = a_0 + \sum_{i=1}^{k} b_i X_i + \sum_{i,j}^{k} b_{ij} X_i X_j, \tag{5}$$

where a_0 is the free term of the regression equation, the coefficients b_1, b_2,…b_k and b_{12}, b_{13}, …b_{kk} are the linear and the interaction terms, respectively. Xi represents input parameters (d, P and V). The output (residual stresses σ_s and σ_d) is also called the response factors.

The experimental plan and result of the trials is reported in *Table 2*. Based on 3^3 full factorial design, a total of 27 tests were carried out. The range of each parameter is set at three different levels, namely particle sizes, laser power and scan speed.

5.2 Experiments design

The plan of tests was developed with the aim of relating the influence of particle sizes (μm), laser power (W) and scan speed (mm/s), with the residual substrate stress σ_s and residual deposit stress σ_d. *Table 4* shows all values of residual stresses σ_s and σ_d. The residual stresses σ_s and σ_d were obtained in the range of 200 – 440; -220 – -90 MPa for σ_s and σ_d.

Table 2: Experimental plan and results

N°	Input parametric			Output responses	
	***d*, µm**	***P*, W**	***V*, mm/s**	**σ_s, MPa**	**σ_d, MPa**
1	20	1600	5.5	220	-115
2	20	1600	6.6	210	-110
3	20	1600	9	200	-90
4	20	1800	5.5	235	-120
5	20	1800	6.6	220	-115
6	20	1800	9	205	-109
7	20	2000	5.5	250	-135
8	20	2000	6.6	235	-120
9	20	2000	9	220	-122
10	60	1600	5.5	300	-145
11	60	1600	6.6	285	-140
12	60	1600	9	270	-125
13	60	1800	5.5	345	-160
14	60	1800	6.6	325	-155
15	60	1800	9	305	-130
16	60	2000	9	310	-145
17	60	2000	5.5	360	-180
18	60	2000	6.6	340	-170
19	100	1600	9	375	-170
20	100	1600	6.6	385	-180
21	100	1600	5.5	400	-200
22	100	1800	9	380	-175
23	100	1800	6.6	390	-172
24	100	1800	5.5	425	-210
25	100	2000	6.6	420	-210
26	100	2000	5.5	440	-220
27	100	2000	9	400	-200

5.3 Analysis of variance ANOVA

The statistical significance of the fitted quadratic models was evaluated by the Prob. values of ANOVA. In the ANOVA table, the sum of squares is used to estimate the square of deviation from the significant mean. Mean squares are estimated by separating the sum of squares by degrees of freedom. F ratio is an index used to check the suitability of the model in which the calculated value of F should be greater than the F-table value. F-table value corresponding 95% confidence level in calculation of process parameters accurately is

$F_{0.05,\ 1,\ 20} = 4.35$. The model is suitable at a 95 % confidence level because the calculated F value is greater than the F value from the table. When the Prob. values are <95 % confidence (0.05), the models achieved are considered

statistically significant. The Design-Expert (State-Ease, version 8) software was used for a statistical analysis of experimental data and to generate the response surface. *Table 3* shows that the particle sizes (d, μm) have the statistically most significant influence on the residual substrate stress σ_s followed by laser power (P, W) and scan speed (V, mm/s), their contributions being (3.68 and 3.29) %, respectively. The interactions ($d \times P$), ($d \times V$) and ($P \times V$) are not significant. Respectively, their contributions are (0.03; 0.04 and 0.11) %. The determination coefficient model's R^2 is 0.9896. The Pred. R^2 of 0.9834 is in reasonable agreement with the Adj. R^2 of 0.9864. The equation in terms of real factors is given as follows:

$$\sigma_S = -40{,}922 + 1{,}991d + 0{,}151P + 11{,}660V + 0{,}00026d \times P - 0{,}029d \times V - 0{,}011P \times V \quad (6)$$

Table 3: ANOVA of residual substrate stress σ_s

Source	Sum of squares	DF	Mean square	F-value	Prob.	Cont. %	Remarks
Model	157155.003	6	26192.500	315.960	< 0.0001		Significant
d, μm	141843.108	1	141843.108	1711.056	< 0.0001	92.85	Significant
P, W	5625.144	1	5625.144	67.856	< 0.0001	3.68	Significant
V, mm/s	5022.951	1	5022.951	60.592	< 0.0001	3.29	Significant
$d \times P$	52.083	1	52.083	0.628	0.4373	0.03	Not significant
$d \times V$	55.046	1	55.046	0.664	0.4247	0.04	Not significant
$P \times V$	174.921	1	174.921	2.110	0.1618	0.11	Not significant
Error	1657.959	20	82.897				
Total	158812.963	26				100	
SD = 9.104					R^2 = 0.9896		
Mean = 312.963					R^2 Adjusted = 0.986		
Coefficient of variation = 2.909					R^2 Predicted = 0.983		
Predicted residual error of sum of squares (PRESS) = 2638.9726					Adequate precision = 53.471		

The ANOVA results of residual deposit stress σ_d presented in Table 4 show that the most significant model term is the particle sizes (d) with 82.78 % of contribution, followed by P with lower contribution of 8.94 %. The term V appears especially significant on thrust force. Its contribution is 7.95 %. On the opposite side, the interactions ($d \times P$), ($d \times V$) and ($P \times V$) are not significant. Respectively, their contributions are (0.08; 0.22 and 0.02) %. The coefficient R^2 of about 0.9631 is considered good, but the Pred. R2 of 0.9283 which represents the efficiency of the model to expect new runs is not as close to the Adj. R2 of 0.9520. The equation in terms of real factors resulted from the backward elimination process is given as follows:

$$\sigma_d = -55{,}521 - 0{,}874d - 0{,}037P + 8{,}31V - 0{,}00018d \times P + 0{,}0339d \times V - 0{,}0021P \times V \quad (7)$$

Table 4: ANOVA of residual deposit stress σ_d

Source	Sum of squares	DF	Mean square	F-value	Prob.	Cont. %	Remarks
Model	32794.411	6	5465.735	86.949	< 0.0001		Significant
d, µm	26310.995	1	26310.995	418.558	< 0.0001	82.78	Significant
P, W	2841.184	1	2841.184	45.197	< 0.0001	8.94	Significant
V, mm/s	2527.234	1	2527.234	40.203	< 0.0001	7.95	Significant
d×*P*	27	1	27	0.429	0.5197	0.08	Not significant
d×*V*	70.795	1	70.795	1.126	0.3012	0.22	Not significant
P×*V*	6.604	1	6.604	0.105	0.7492	0.02	Not significant
Error	1257.218	20	62.860				
Total	34051.629	26				100	
SD = 7.928					R^2 = 0.9631		
Mean = -152.703					R^2 Adjusted = 0.952		
Coefficient of variation = 5.1921					R^2 Predicted = 0.928		
Predicted residual error of sum of squares (PRESS) = 2441.888					Adequate precision = 31.180		

The predicted values of response factors illustrating residual substrate stress σ_s and residual deposit stress σ_d, from regression Eqs. (6) – (7) corresponding to different combinations of input parameters, are reported in *Table 2*.

Fig. 8 shows the comparison between the predicted and measured values of residual substrate stress σ_s and residual deposit stress σ_d. It is concluded that the results of the comparison prove that predicted values of the residual stresses (σ_s and σ_d) are very close to those determined experimentally.

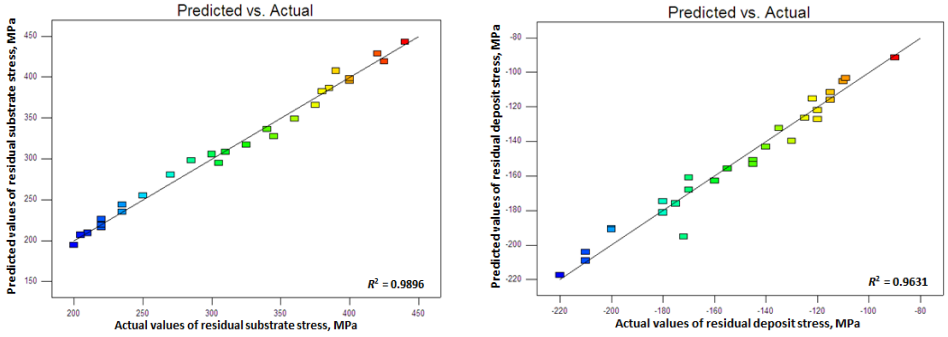

Figure 8: Comparison between measured and predicted values for residual stresses (σ_s and σ_d).

Fig. 9 represents a perturbation plot for the (σ_s and σ_d), in which the line represented by the different factors, particle sizes (A), laser power (B) and scan speed (C) revealed their individual behaviors on (σ_s and σ_d), respectively, keeping other parameters constant. *Fig. 8* depicts an increasing trend of residual stresses by increasing the particle sizes (A), where as a decreasing trend with increase in scan speed (C).

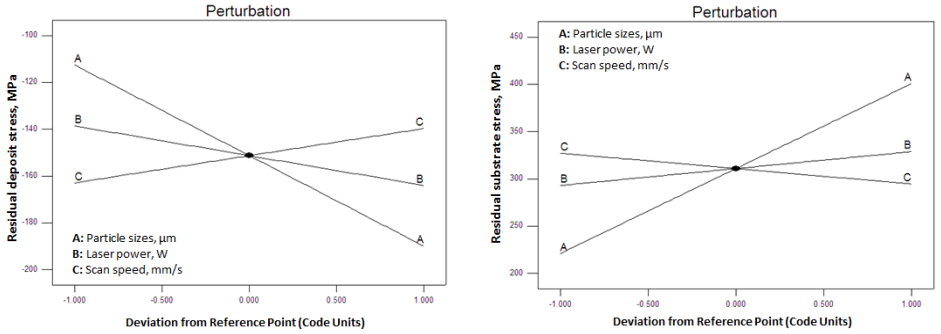

Figure 9: Effect of input parameters on σ_s and σ_d.

In order to investigate the influence of the scan speed and laser power parameters at various particle sizes on the residual stresses (substrate stress σ_s and deposit stress σ_d), response surface is drawn in *Fig. 10*. Fig. 10 depicts he influence of scan speed (V) and laser power (P) on the residual stresses (stress σ_s and σ_d), reported before. The highest residual stresses are achieved with the combination of the highest scan speed and the highest laser power when the particle sizes (d) are kept at high level.

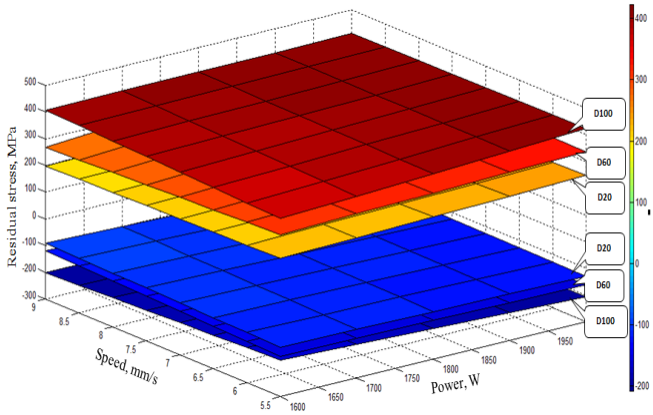

Figure 10: Effect of the scan speed and laser power on the resudial stresses.

5.4 Optimization of input conditions

In the present study, the desired function optimization of the RSM has been employed for residual substrate and deposit stress optimizations using Design Expert Software. The goals and the parameter ranges defined for the optimization process are summarized in *Table 5* for minimizing the values of the residual stresses (substrate stress σ_s and deposit stress σ_d). The desirability levels are constant up to solutions no. 8. After these solutions (*Table 6*), the desirability levels decrease hen the operating parameter is changing. So, we can conclude that in the case of the highest particle sizes, highest laser power and lowest scan speed, the performances of the deposit are optimized and the desirability levels are (83.65 and 83.23) % in these conditions.

Table 5: Constraints for optimization of deposit conditions

Condition	**Goal**	**Lower limit**	**Upper limit**
Particle sizes, d(μm)	Is in range	20	100
Laser power, P (W)	Is in range	1600	2000
Scan speed, V (mm/s)	Is in range	5.5	9
σ_s (MPa)	Minimize	200	440
σ_d (MPa)	Minimize	-220	-90

Table 6: Response optimization for residual substrate and deposit stress

Test n°	d	P	V	**Residual stress**		**Desirability**
	(μm)	(W)	(mm/s)	σ_s (MPa)	σ_d (MPa)	
1	100.00	2000.00	5.50	348.878	-217.356	0.8365
2	100.00	1999.96	5.53	348.579	-217.158	0.8359
3	100.00	2000.00	5.54	348.403	-217.042	0.8355
4	100.00	1994.31	5.50	348.262	-216.971	0.8353
5	100.00	1991.73	5.50	347.985	-216.799	0.8348
6	100.00	2000.00	5.58	347.951	-216.744	0.8346
7	100.00	1987.81	5.50	347.561	-216.534	0.8340
8	100.00	2000.00	5.67	346.881	-216.038	0.8323

6. Conclusion

Based on a study of the influence of powder particle size on the characteristics of coatings the following conclusions are made:

- Absorption of beam laser energy is a much localized surface phenomenon.

- Reducing particle sizes leads to an increase in the resulting laser absorption.
- Small particles sizes form a dense screen with the appearance of a multiple scattering phenomenon which absorbs very efficiently the incident laser beam.

Consequently, the laser energy density may be reduced and good morphological aspects of claddings with an optimal dilution, enough to create good metallurgical bond, can be obtained. In addition, low levels of residual stresses can be obtained because of thermal gradients attenuation. Further, experiments are in progress to study the case of very small particle sizes, especially by using spherical shape particles of uniform diameter.

- Also, the results of ANOVA and the validation experiments confirm that the developed mathematical model shows excellent fit and predicted values are very close to experimental values.
- The residual substrate stress (σ_s) and residual deposit stress (σ_d) are influenced principally by the particle sizes factor with contribution of (82.78 and 92.85) %, respectively.

7 References

[1] Yakovlev, A., Bertrand, P., and Smurov, I., "Laser Cladding of Wear Resistant Metal Matrix Composite Coatings", *Thin Solid Films*, v. 453-454, pp. 133-138, 2004.

[2] Pei, Y.T., Ouyang, J.H., and Lei, T.C., "Microstructure of bonding zones in laser-clad Ni-alloy-based composite coatings reinforced with various ceramic powders", *Surf. Metall. Mater. Trans*, vol. 27A2, pp. 391-400, 1996.

[3] Hidouci, A., Pelletier, J.M., Ducoin, F., Dezert, D., and El Guerjouma, R., "Microstructural and mechanical characteristics of laser coatings", *Surface and Coatings Technology*, vol. 123, pp. 17-23, 2000.

[4] Safonov, A.N., and Aleksenko, S., „Effect of laser treatment on the wear resistance of steels", *Metal Science and Heat treatment*, vol. 40, pp. 399-401, 1998.

[5] Sexton, C.L., Byrne, G., and Walkins, K.G., "Alloy development by laser cladding: an overview", *Journal of Laser Applications*, vol. 13, pp. 2-11, 2001.

[6] De Oliveira, U., Ocelik, V., and De Hosson, J.T.M., "Analysis of coaxial laser cladding processing conditions", *Surface and Coatings Technology*, vol. 197, pp. 127-136, 2005.

[7] Sallamand, P., "Alliage de surface et revétements élaborés sous faisceau laser par projection de poudre sur substrat base aluminium: caractërisation microstructurale, mécanique et tribologique",. *Thesis*, INSA de Lyon, 1994.

[8] Pelletier, J.M., Sahour, M.C., Pilloz, M., and Vannes, A.B., "The Influence of processing conditions on geometrical features of laser claddings obtained by powder injection", *Journal of Materials Science*, vol. 28 (19), pp. 5184-5188, 1993.

[9] Jackson, M.J., and O'Neill, W., "Laser micro-drilling of tool steel using Nd:YAG lasers", Journal of Materials Processing Technology, vol. 142 (2), pp. 517-525, 2003.

[10] Laracine, M., Bignon, C., Lormand, M., Vannes, A.B., and Bedrin, C., "Determination of residual stresses in multimaterial, multilayer pieces : adaptation to ceramic coatings", *CIRP Annals*, vol. 40, pp. 535-539, 1991.

[11] Laribi, A., Mesrati, N., Vannes, A.B., and Treheux, D., "Adhesion and residual stresses determination of thermally sprayed molybdenum on steel", *Surface and Coating Technology*, Elsevier, vol. 166, pp. 206-212, 2003.
[12] Flavenot, J.F., "Mesure des Contraintes Résiduelles: Methode de la Flêche - Methode de la Source des Contraintes", *Les mémoires techniques du CETIM*, vol. 31, 1977.
[13] De, A., and DebRoy, T., "A smart model to estimate effective thermal conductivity and viscosity in the weld pool", *Journal of Applied Physics*, vol. 95 (9), pp. 5230-5240, 2004.
[14] Monagham, B.J., Neale, J.G.J., and Chapman, L., "Some Thermal Properties of a Copper–Tin Alloy", International Journal of Thermophysics, Springer, vol. 20 (4), pp. 1051-1060, 1999.
[15] Touloukian, S., and Dewitt, D.P., Thermophysical Properties of Matter, Vol. 8, p. 31, IFI/Plenium New York, N.Y. 1972.
[16] Aouici, H., Yallese, M.A., Chaoui, K., Mabrouki, T., and Rigal, J.-F., "Analysis of surface roughness and cutting force components in hard turning with CBN tool: prediction model and cutting conditions optimization", *Measurement,* vol. 45, pp. 344–353, 2012.